Single-Pass Laser Beam Welding of Clad Steel Plate

Trials show the possibility of a satisfactory composition and crack-free weld metal

BY S. MISSORI, F. MURDOLO, AND A. SILI

ABSTRACT. The possibility of laser beam welding (LBW) clad steel plates in one pass with a single filler metal was investigated. Two procedures, one with a single-side laser beam and the other with a dual-beam laser, were utilized for butt-joint welding of carbon steel plates clad with austenitic stainless steel. Filler metal was in the form of strips, interposed within edges prior to welding. Metallographic observations and X-ray energy dispersive spectroscopy microanalysis were performed on welded specimens. Mechanical properties were evaluated by Vickers microhardness and tensile tests. These investigations have shown the possibility of making sound welds with a satisfactory composition and crack-free weld metal with both experimental procedures.

Introduction

Plates or tubes of carbon or low-alloy steel clad with an alloyed material are an economical solution to meet the increasing demand of industrial processes for combining elevated strength with good corrosion resistance. Both base steels and cladding materials can be selected from a large variety according to specific requirements and operations. The available base steels include structural steels, pressure vessel steels for elevated temperature, and fine-grained steels. Cladding materials are provided in several classes of stainless steels, nickel alloys, copper alloys, or titanium alloys.

Cladding materials are normally applied to base steels by explosion welding, weld surfacing, solid-state welding by coextrusion, or hot rolling, obtaining strong metallurgical bonding at the interfaces. Cladding thickness may vary from 5 to 50% of the total thickness, but it is generally 10 to 20% for most applications (Ref. 1). This advantageous combination gives rise to a remarkable reduction in weight and cost savings in comparison with the utilization of solid plates.

In our experiments, we considered one of the most usual cases, that of carbon steel clad with stainless steel. It is important to remark that due to adverse metallurgical reactions, the welding techniques described below can by no means be applied to plate clad with titanium or other nonferrous alloy materials. Usually, welding of plate clad with stainless steel is carried out by arc welding processes (manual arc, submerged arc, gas metal arc, or gas tungsten arc welding). The conventional welding techniques require the following steps to be undertaken (Refs. 1–3):

1) the base steel is first welded with a filler metal;

2) the steel weld is backgouged to the sound metal, producing a groove;

3) welding of clad material can start with deposition of one or several buffer layers by using a filler metal higher alloyed than the cladding metal in order to form a layer that is tolerant of some dilution with the base metal;

4) welding is completed with filler and cover layers of cladding-like weld metal.

This welding procedure requires a quite complex practice including the use of different types of filler metals; moreover, the number of passes is the sum of passes required to weld base steel and cladding material separately plus the additional passes due to backgouging. Normally, many passes are required. Thus, it is advantageous to investigate the possibility of reducing the number of passes by high-penetration LBW. In particular, our work deals with butt-joint welding of carbon steel plates clad with stainless steel by single-pass LBW. Both single-side and dual LBW procedures were considered. Filler metal was in the form of strips or consumable inserts. It is well known that consumable inserts of several configurations (inverted T, Y, rectangular shape, etc.) are often utilized with conventional arc welding for better fitup and easier root welding of components that cannot be back welded from inside (e.g., piping). Particularly in these cases, a welding technique for clad steel that uses a single filler metal could be an interesting solution.

Investigations on welded samples included metallographic observations by optical and scanning electron microscopy (SEM), microanalysis by energy dispersive spectroscopy (EDS), microhardness tests, and tensile tests.

KEY WORDS

Clad Steel
Consumable Inserts
Laser Beam Welding (LBW)
Hot Cracks

Materials and Methods

Materials

The materials utilized in these welding trials were carbon steel plates (6.5 mm thick), clad with a low-carbon austenitic stainless steel (2.5 mm thick). These plates were produced by hot rolling by Voest-Alpine Stahl GmbH, Linz, Austria. The clad thickness was chosen because it was readily available from the supplier. Even though the thickness is a little greater than usual (27.7% of the total thickness), the results obtained can be extended to different thickness ratios provided that the effect of different dilution on the fusion zone (FZ) is properly taken into account in the choice of filler metal composition, as explained afterward in the discussion of results. The base material specification is H II DIN 17155, equivalent to ASTM 515 Gr. 60. The cladding metal specification is 1.4306 DIN 17440, equivalent to AISI 304. The chemical compositions of the two steels are given in Table 1.

The weld metal derives from the fusion of the filler metal and of a portion of base and cladding metals, according to the dilution and melt pool dynamics caused by the welding process. The filler metal was chosen in such a way that the weld metal is suitable to ensure the continuity of the cladding layer and its good anticorrosion properties and, moreover, does not contain structures that might develop undesirable brittleness or cracking after dilu-

S. MISSORI is with Dipartimento Ingegneria Meccanica, Università di Roma, Italy. F. MURDOLO and A. SILI are with Dipartimento Chimica Industriale e Ingegneria dei Materiali, Università di Messina, Italy.

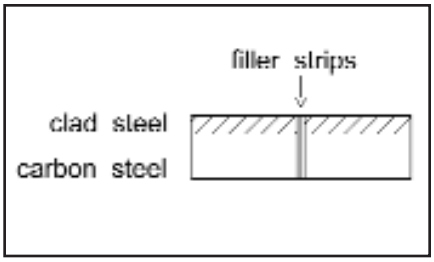

Fig. 1 — Square edge preparation of clad plates.

tion with the steel. Based on results of previous experiments in LBW of dissimilar metals (Refs. 4, 5), two different filler materials have been utilized (Table 2):

a) Nickel-based alloy (DIN 2.4806), which can tolerate high dilution with carbon steel without becoming crack sensitive. In addition, the solubility of carbon is lower by comparison to that in austenitic stainless steel, minimizing carbon migration from the ferritic steel to the weld metal during welding and while in service (Refs. 6–8).

b) Austenitic stainless steel (DIN 1.4465), with the aim of achieving a FZ composition similar to the one of clad stainless steel, free from martensite (to reduce risk of cold cracking), and with little delta ferrite, effective in preventing hot cracking in the austenitic matrix (Refs. 9–13).

Edge Preparations and Welding Processes

Welds in butt joints were performed on plates with square edge preparation, as shown in Fig. 1. The filler metal was put into the joint in the shape of strips. Initially, the LBW techniques were scheduled to utilize either dual laser beam or single laser beam, as well as either nickel-based alloy or austenitic steel alloy filler metal (four techniques in all), but the program could not be completed and, in fact, only the following two techniques were tested:

Procedure A: Dual LBW, with the beams traveling horizontally and the plates being positioned on a vertical plane — Fig. 2. The two laser systems were a unit UTIL 25 kW and a Rofin Sinar SR 170 (nominal power 17 kW). The focusing devices were 35-deg-off-axis paraboloids with a focal length of 682 mm each. Three strips of Ni-based alloy filler metal Type 2.4806, each being 0.4 mm thick (1.2 mm total thickness), were utilized for this procedure.

Procedure B: Single-side LBW with the plates in flat position — Fig. 3. The laser equipment was a unit UTIL 25 kW, DC, with unstable resonator configuration, nonpolarized, using CNC five-axis gantry portal. The focusing device was a 90-deg-off-axis paraboloid with a focal length of 300 mm. Two strips of the austenitic filler metal Type 1.4465 (similar to ER 310Mo), each being 0.5 mm thick (1 mm total thickness), were utilized.

The welding parameters of procedures A and B are given in Table 3. For both procedures, a diagnostic system was utilized before welding to check the features of the laser beam. The estimated Rayleigh lengths are adapted to the thickness of the workpieces. The weld pool protection and the plasma control were performed by a stream of helium gas. No preheating or postweld heat treatments were carried out.

Table 1 — Specifications and Chemical Composition of Plates, from Maker Certificate

Material:	Base: Carbon Steel	Cladding: Stainless Steel
Thickness:	6.5 mm	2.5 mm
DIN Specification:	H II DIN 17155	1.4306DIN17440
ASTM Equiv. Specification:	A 515 Gr. 60	A240 Type 304 L
Chemical Composition (wt-%)		
C	0.145	0.017
Mn	0.85	1.32
Si	0.20	0.39
P	0.008	0.029
S	0.001	0.003
Al	0.04	—
Cr	—	18.39
Ni	—	10.07

Table 2 — Specifications and Chemical Composition of Filler Metals, from Maker Certificate

Specification:	DIN 2.4806	DIN 1.4465
Other Designation:	AWS ERNiCr3	AWS ER310Mo Modified
Thickness:	0.4 mm	0.5 mm
Chemical Composition (wt-%)		
C	0.020	0.010
Mn	3.00	6.00
Cr	20.50	25.00
Si	0.10	0.10
Ni	bal.	22.6
Mo	—	2.10
Nb	2.50	0.01
Fe	1.5	bal.

Table 3 — Welding Parameters

	Procedure A Dual LBW	Procedure B Single-Side LBW
Power at the Workpiece:	2⟨ 10.0 kW	10.0 kW
Welding Speed:	3.0 m/min	1.6 m/min
Distance Δz:	0 mm	–1 mm
F-Number:	10/8	4
Focal Radius:	530/342 µm	250 µm
Helium Flow Rate:	2⟨ 25 L/min	20 L/min
Filler Metal:	N.3 strips ERNiCr3 alloy (0.4 mm thick)	N.2 strips ER310Mo modified (0.5 mm thick)
Position:	Plates on vertical plane with two laser beams traveling horizontally.	Plates on horizontal plane with laser beam on the clad side.
Edge Preparation:	Squared	Squared

Metallurgical Investigations

The welded plates were cut transversely to the bead to obtain samples of the welded sections. Metallographic spec-

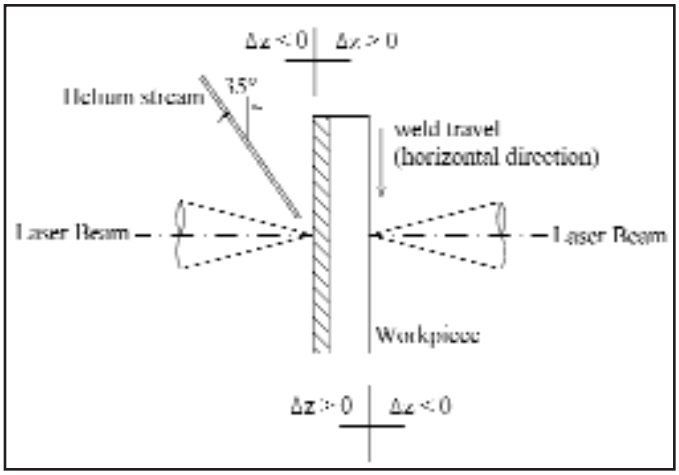

Fig. 2 — Dual LBW procedure assembly.

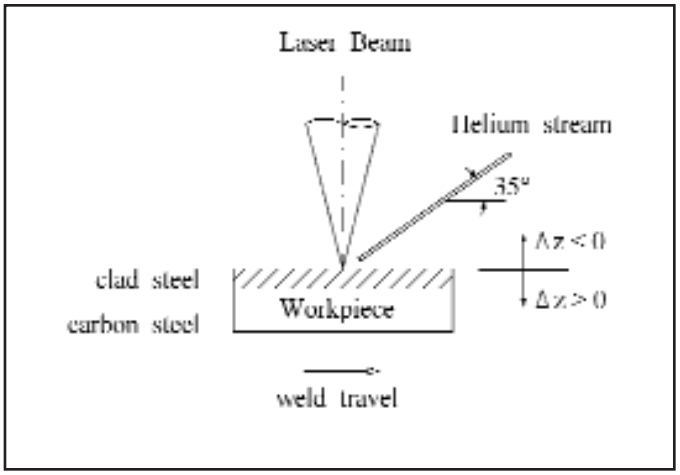

Fig. 3 — Single-side LBW procedure assembly.

imens were prepared by conventional mechanical polishing and then etched by 2% Nital or Glyceregia to reveal carbon steel and austenitic microstructures. The following experimental work was performed:

Visual inspection and macrographic examination. Welds were submitted to visual and macrographic inspection. A minimum of three macrographic samples per each procedure were cut and examined.

Optical and SEM metallurgical observations of the FZ and HAZ.

Microanalysis by energy dispersive spectroscopy (EDS). Variations in composition along the centerline of the weld zone were analyzed by a electron probe, Type JSM-35 CF, equipped with an energy dispersive spectrometer, Model EDAX 711, at an accelerating voltage of 15 kV. The analysis was performed on samples taken from both welding procedures. The content of the elements mainly influencing the formation of phases, in particular Cr and Ni, was quantitatively measured in at least ten points, located on a traverse along the weld zone crossing the full thickness of the sample.

Evaluation of fusion zone areas. The survey of the dimensions of each cross section of the welds was performed with the aid of an optical microscope by measuring the coordinates of the profile of the melt zone, divided in slices of equal height, and evaluating the area by a numerical method.

Estimation of microstructures by Schaeffler diagram (Ref. 14). The contents of Cr and Ni were taken as estimated by SEM microanalysis. Carbon and Mo contents were calculated from base and filler metal compositions, taking account of the dilution and the actual contribution of each material (base metal and filler metal) to the formation of the FZ, according to its respective melted area.

Microhardness tests. Vickers microhardness tests (100-g load, 10-s time) on metallographic samples. Microhardness values were measured on:

• a first traverse along the centerline of FZ;

• a second traverse in the middle of the clad steel thickness, parallel to the clad line;

• a third traverse in the middle of the base carbon steel thickness, parallel to the clad line.

Consequently, three hardness profiles were obtained for each welded sample.

Tensile tests. Tests were performed on specimens cut normally to the welding direction, in order to evaluate the tensile strength of welded joints. Two specimens per each welding procedure were provided.

Table 4 — Tensile Test on Welded Samples

Welding Procedure	Tensile Strength (MPa)	Failure Zone
Dual LBW	486	Base metal
	479	
Single-Side LBW	468	HAZ
	463	

Results

Visual Inspections and Macrographic Examinations

Figure 4A and B shows representative macrographs of the welded sections obtained with the two LBW procedures. Both samples showed a satisfactory appearance. No major discontinuities, such as cracks and incomplete fusion, were observed. Both welding procedures gave rise to a good bridgeability. On the sample welded with dual LBW, little porosity was observed, but no quantitative evaluation was made of size and number of pores.

In order to evaluate the extension of the FZ and heat-affected zone (HAZ), the macrographic cross-sectional areas were measured with the aid of an optical microscope. In Fig. 5 A and B, the welded sections are sketched with the indications of the FZ and HAZ sizes. No metallurgical changes were observed in the clad steel near the fusion boundary. Samples obtained by the single-side LBW procedure show a smaller extension of the FZ and HAZ.

Tensile Tests

Tensile tests show a good mechanical soundness for both procedures. The results of tensile tests on two samples per each procedure are reported in Table 4. The tensile strength values are greater than the minimum nominal tensile strength of carbon steel, equal to 410 MPa. Failure took place in the base metal for samples welded by the dual LBW procedure and in the HAZ for the single-side LBW procedure.

Vickers Microhardness Tests

The hardnesses measured on welded sections show similar profiles for both LBW procedures A and B. Representative Vickers microhardness profiles are given in Fig. 6A–C for procedure A and in Fig. 6D–F for procedure B.

a) *Traverse along FZ.* The profiles along the central line of the welded sections are fairly even and are in the range 190–240 HV for procedure A (Fig. 6A) and in the range of 180–200 HV for procedure B (Fig. 6D).

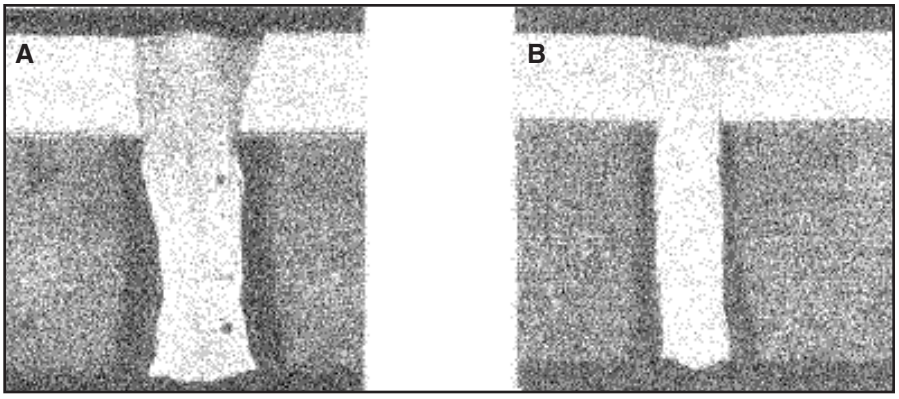

Fig. 4 — Macrographs of welded sections: A — dual LBW; B — single-side LBW.

b) *Traverse along clad steel, parallel to cladding line* (Fig. 6B and E). No significant variation of microhardness occurred along the width of the FZ or in the clad steel near the FZ (variation range of 180–210 HV). Moreover, these microhardness values are of the same order as the initial microhardness of the clad material.

c) *Traverse along carbon steel, parallel to cladding line* (Fig. 6C and F). The hardness profile along the FZ width is quite even, except for some increase in the vicinity of the fusion boundary. In the HAZ, as commonly observed in ferritic steel, the hardness decreases as the distance from the fusion boundary increases. Peak hardness values were measured near the fusion boundary line in the range of 300–400 HV. At distances greater than 3 mm, the hardness stays constant and is equal to that of the unaffected carbon steel (about 150 HV).

Metallographic Observations and Microanalysis by EDS

Microstructures the Base Metals and the Clad Steel/Carbon Steel Interface

The carbon-base steel shows a microstructure consisting of a mixture of grains of ferrite and pearlite, with pearlite disposed in longitudinal bands, typical of milled products. As pointed out in a previous work (Ref. 15), a carbon migration from the base steel toward the stainless austenitic steel occurs during the fabrication process of clad plates due to the hold time at high temperature. The carbon diffusion gives rise to microstructural changes in the two steels, near the bimetallic interface or cladding line (Fig. 7). This interface is clearly detectable as a narrow band, less than 10 μm wide. At the carbon steel side, a decarburized region about 120 μm wide, without pearlite and with ferritic grains larger than ones far from the interface, can be observed. The austenitic side is characterized by a precipitation zone, ~200 μm wide, where precipitated alloy carbides are clearly visible. In particular, the carbide concentration gradually decreases as the distance from the cladding line increases. Energy dispersive spectroscopy measurements on traverses across the cladding line have shown diffusion profiles of substitutional elements centered around the cladding line and interesting small distances of about 20 μm (Ref. 15). Welding operations do not appear to affect this initial condition.

Microstructures of the HAZ

During welding, the region closest to the weld interface undergoes a fast heating at a temperature exceeding the Ac_3 point (ferrite-austenite transformation). Consequently, complete or partial austenitization with different homogeneity of austenite occurs in the carbon steel at several distances from the weld interface, according to nucleation and growth controlled by the temperature/time history of each portion of steel. Furthermore, the subsequent microstructural transformations vary according to the cooling rate at the several distances from the weld interface.

With reference to a sample welded with procedure A, on the carbon steel side, the HAZ, less than 0.8 mm wide, is characterized by:

- first a narrow zone near the weld interface where a hard structure, probably a bainite + martensite mixture, with a microhardness peak of about 400 HV can be observed (Fig. 8);
- a second zone with greater width in which hardening structures are present mixed with untransformed ferrite (Fig. 9) with intermediate values of microhardness (200–250 HV). The amount of untransformed ferrite increases gradually with the distance from the weld interface. The microhardness decreases down to about 150 HV in the unaffected zone.

In the clad steel near the FZ, there is no evidence of structural transformations.

Microstructures of FZ

Figure 10 gives the concentration profiles of Ni and Cr by EDS measurements in the FZ along the joint thickness. The highest Ni and Cr concentrations are reached in the FZ of samples obtained with the dual-beam laser welding procedure, utilizing a high-nickel alloy as filler metal. With the single-side procedure, the alloy element concentrations in the FZ gradually decrease along the joint thickness, from the austenitic clad metal to the carbon steel side. In both procedures, metallographic observations have shown a crack-free, austenitic microstructure in

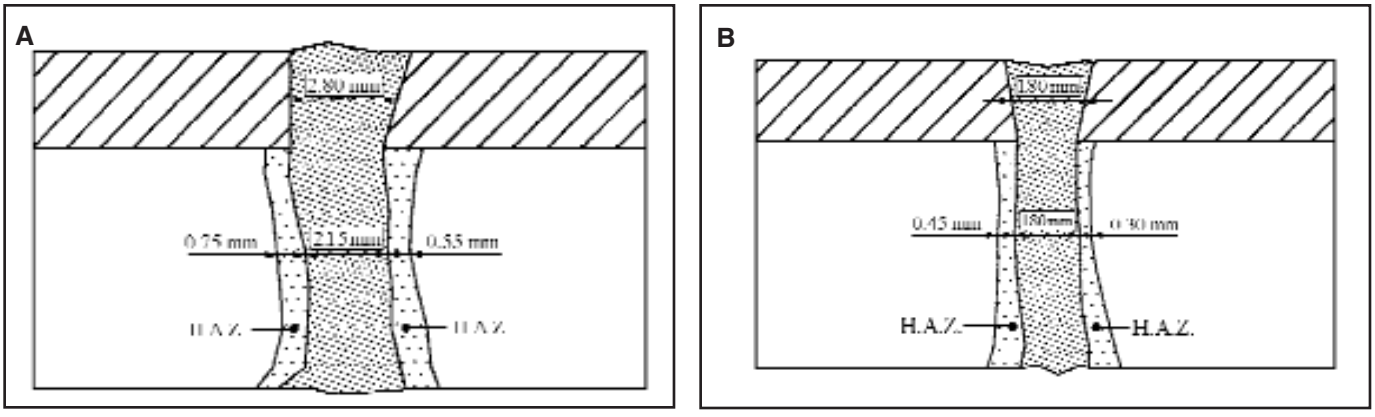

Fig. 5 — Sketches of the welded sections: A — dual LBW; B — single-side LBW.

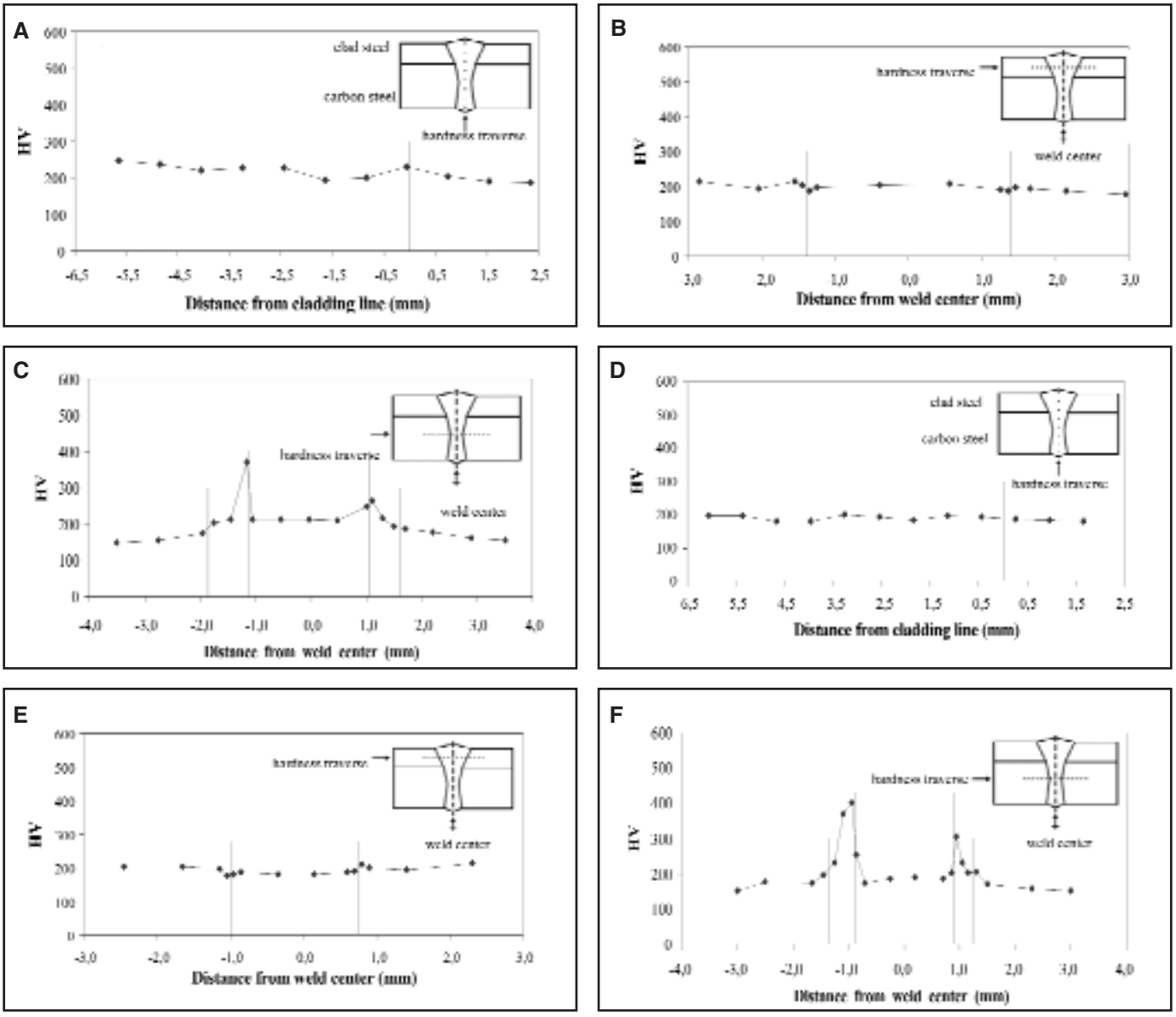

Fig. 6 — Microhardness profiles in welded sections: A, B, C — dual LBW; D, E, F — single-side LBW.

the FZ, along all the thickness of the joints. In particular, the FZ has the following characteristics according to the welding procedures utilized:

- procedure A, dual LBW: an austenitic microstructure, with high-nickel alloy composition, fairly homogeneous, with some precipitates at the grain boundary (Fig. 11);
- procedure B, single LBW: an austenitic microstructure with alloy composition close to the austenitic clad steel (Fig. 12).

Discussion

The phases in the FZ have been estimated by reporting microanalysis measurements as points on a Schaeffler diagram.

The dual-beam LBW (procedure A), which utilizes a Ni-based alloy as filler metal, gives rise to a quite homogeneous composition of the fusion zone along all the thickness, resulting in a fully austenitic phase. All the points representative of the FZ composition are in the austenitic region, typical of the alloys with high Ni composition (Fig. 13). The microhardness values are relatively low. The evaluation of average composition based on SEM microanalysis agrees with the determination based on dilution of fusion zones and material compositions. However, the Cr content, estimated by EDS, decreases along the thickness from 16% (clad steel side) to 12% (carbon steel side). Ni content is more homogeneous and is in the range of 35–40%. According to the results of microhardness tests, showing an even transversal profile, it appears reasonable to suppose that no anomalies due to incomplete mixing out of the FZ centerline should be present all along the width.

The single LBW (procedure B) with the use of filler metal Type ER 310Mo/modified shows a composition of FZ with both Cr and Ni decreasing a little along the thickness going from the clad steel to the carbon steel side. Chromium goes from 18 to 14% and Ni from 14 to 11%. On the Schaeffler diagram (Fig. 14), the points representative of Ni and Cr equivalent compositions along the weld thickness are still in the austenitic field. In particular, the points related to the compositions of the FZ at the carbon steel side fall at the boundary between the austenitic and the austenitic–martensitic regions. In any case, composition and microstructure can be considered satisfactory for this procedure as well. The hardness values are relatively low with an even profile along the fusion zone, confirming the phase estimation ac-

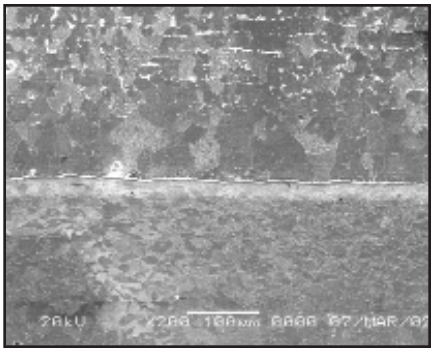

Fig. 7 — Micrograph of the bimetallic interface.

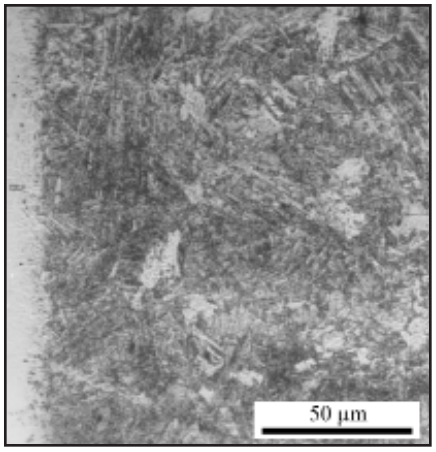

Fig. 8 — Micrograph of the carbon steel HAZ region with high hardness.

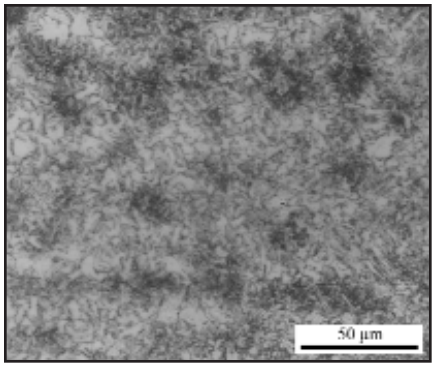

Fig. 9 — Micrograph of the carbon steel HAZ region with low hardness.

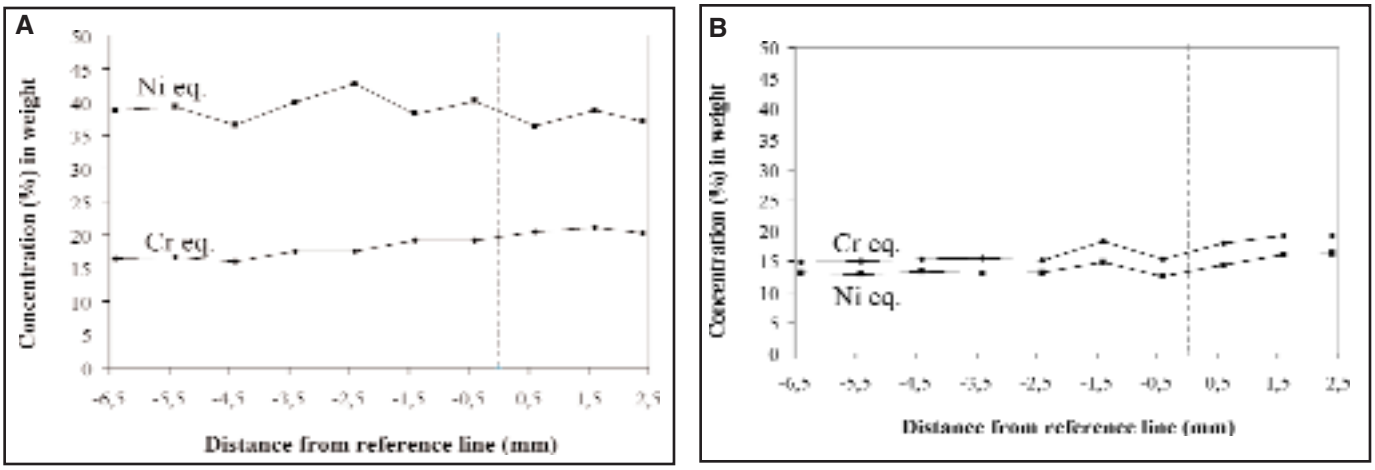

Fig. 10 — Ni and Cr concentration profiles in welded sections: A — dual LBW; B — single-side LBW.

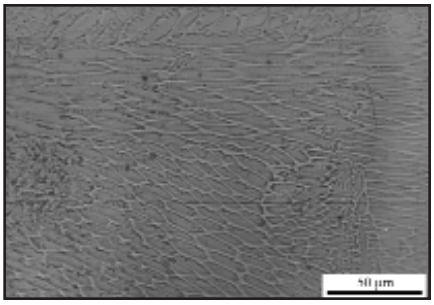

Fig. 11 — Micrograph of the FZ: dual LBW.

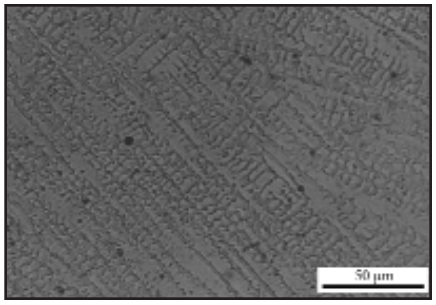

Fig. 12 — Micrograph of the FZ: single-side LBW.

cording to the Schaeffler diagram and the absence of martensitic structures.

The results obtained with the two procedures A and B are not easily compared, due to the different compositions of filler metal and different welding techniques (single or dual LB). It appears, however, that dual LBW offers more capability to fit to geometrical inaccuracies in joint preparation — also thanks to a slightly wider FZ. Moreover, the FZ composition is more even along the thickness.

Tensile tests showed good mechanical soundness of welded joints for both procedures A and B. It was found that all the welded specimens have an ultimate tensile strength not less than the minimum nominal tensile strength of the carbon steel. The failure zone is located in the base metal, out of the FZ. Therefore, the results can be considered satisfactory.

The relatively high values of hardness found in the carbon steel HAZ may be reduced by preheating and/or postweld heat treatment.

As noted in the introduction, the available clad thickness was about 27.7% of the total thickness. However, the clad thickness is usually in the range of 10–20% of the total plate thickness. To successfully apply the welding techniques tested here to cases of smaller ratios of cladding/total thickness, one should consider that the small reduction of alloy element content in the FZ, resulting from a greater contribution of carbon steel to its formation, can be easily compensated by a slightly higher Cr-Ni content in the filler metal. Under this condition, the little divergence from usual clad thickness ratio should not influence the applicability of the welding techniques.

A further improvement of the quality of fusion zones could be expected by using more appropriate filler materials, not readily available at present, to be especially provided for LBW. In particular, for single-side LBW (procedure B), filler material should have a composition slightly

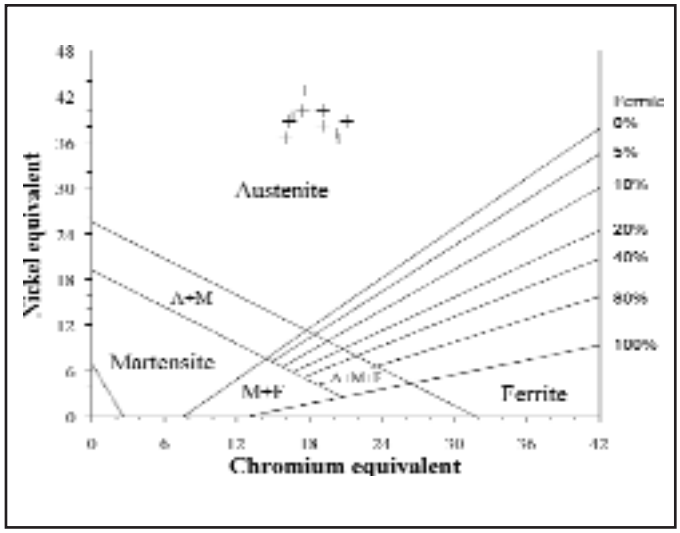

Fig. 13 — Procedure A (ERNiCr3 dual LBW procedure). Schaeffler diagram with points (+) representative of Ni and Cr equivalent compositions in the FZ.

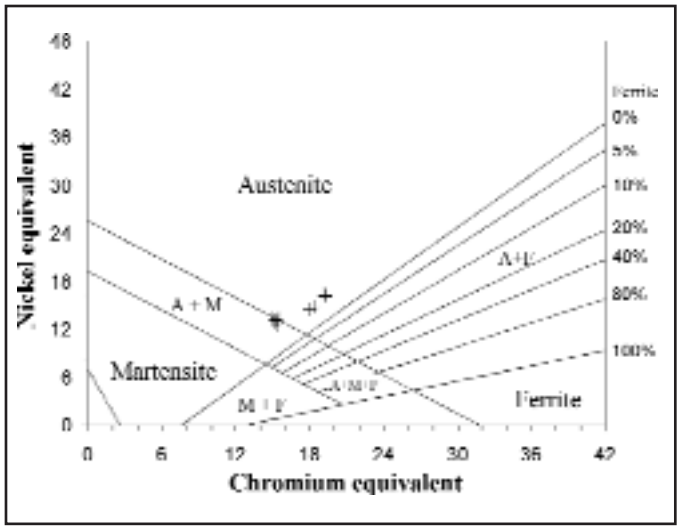

Fig. 14 — Procedure B (ER310Mo modified single-side LBW procedure). Schaeffler diagram with points (+) representative of Ni and Cr equivalent compositions in the FZ.

richer in Cr in order to better compensate for the greater dilution occurring in the base metal carbon steel side. Furthermore, for both procedures, the thickness of the filler metal strips should be increased to make possible the use of a single strip, instead of a number of packed strips. This should improve the heat flow conditions from the weld pool to the base metal and reduce the risks of incomplete fusion or penetration.

Conclusions

It is possible to draw the following conclusions:

a) Both experimental LBW procedures, named A and B, gave promising results for welding clad steel plates by a single pass as it appears feasible to weld clad steel with a satisfactory composition and crack-free FZ.

Procedure A. The dual LBW procedure showed the possibility of performing sound welds in a single pass, obtaining a homogeneous structure with high Ni content.

Procedure B. Metallographic samples of welds showed a quite homogeneous composition of the FZ all along the thickness, close to that (fully austenitic) of the clad steel. The small difference of composition between the portion of the FZ contiguous to clad metal and that contiguous to the carbon-steel metal may be compensated for by a proper increase of Cr content in the filler metal.

b) The results obtained with the procedures A and B are not easily compared, due to the different compositions of filler metal and different welding techniques (single or dual LB). It appears, however, that dual LBW offers more capability to fit to geometrical inaccuracies in joint preparation, due also to a slightly wider FZ. Moreover, the FZ composition is more even along the thickness, thus giving rise to a more homogeneous microstructure.

c) In the FZ obtained by both experimental procedures, moderate and uniform hardness values were exhibited. Mechanical strength of the joints was in all cases greater than the nominal strength of the base carbon steel.

d) The results encourage further experiments to improve the adopted welding techniques, with the aim of optimizing the composition of filler metal, with possible utilization of integral thicker filler strips.

Acknowledgments

The authors thank the Laser Welding Department of Fraunhofer Institut ILT-Aachen for its support in setting up welding procedures and providing technical assistance.

References

1. Oates, W., and Saitta, A., eds. 1998. *Welding Handbook 8th ed., Vol. 4,* pp. 370–371. Miami, Fla.: American Welding Society.

2. Funk, W. H. 1960. *Interpretative Report on Welding of Nickel Clad and Stainless Clad, Bulletin 61.* New York: Welding Research Council.

3. Voest-Alpine Stahl. 1997. *Clad Plates Catalogue.* Linz, Austria.

4. Missori, S., and Koerber, C. 1997. Laser beam welding of austenitic-ferritic transition joints. *Welding Journal* 76(3): 125-s to 134-s.

5. Missori, S., and Koerber, C. 1998. Procedure development for improved quality single and dual LBW of dissimilar metals. *Welding Journal* 77(6): 232-s to 238-s.

6. Klueh, R. L., and King, J. F. 1982. Austenitic-ferritic weld-joint failures. *Welding Journal* 61(9): 302-s to 311-s.

7. Viswanathan, R. 1985. Dissimilar metal welds in service and boiler creep damage evaluation for plant life extension. *Journal of Pressure Vessels Technology* 107: 218–225.

8. Roberts, D. I., Ryder, R. H., and Viswanathan, R. 1985. Performance of dissimilar welds in service. *Journal of Pressure Vessels Technology* 107: 247–254.

9. Brooks, J. A., Thompson, A. W., and Williams, J. C. 1984. A fundamental study of the beneficial effects of delta ferrite in reducing weld cracking. *Welding Journal* 63(3): 71-s to 83-s.

10. Singh, J., Purdy, G. R., and Weatherly, G. C. 1985. Microstructural and microchemical aspects of the solid-state decomposition of delta ferrite in austenitic stainless steels. *Metallurgical Transactions A* 16A(8): 1363–1369.

11. Kujanpaa, V. P., David, S. A., and White, C. L. 1986. Solidification cracking, formation of hot cracks in austenitic stainless steel welds. *Welding Journal* 65(8): 203-s to 212-s.

12. David, S. A., Vitek, J. M., and Hebble, T. L. 1987. Effect of rapid solidification on stainless steel weld metal microstructures and its implications on the Schaeffler diagram. *Welding Journal* 66(10): 289-s to 302-s.

13. Vitek, J. M., and David, S. A. 1988. The effect of cooling rate on ferrite in Type 308 stainless steel. *Welding Journal* 67(5): 95-s to 102-s.

14. Schaeffler, A. L. 1949. Constitution diagram for stainless steel weld metal. *Metal Progress* 56(11): 680–680B.

15. Missori, S., and Sili, A. 1997. Metallurgical transformations on hot rolled clad steel. *Proceedings of EUROMAT 97, Maastricht* 4:51–55.